Desalination and Water Treatment
www.deswater.com

doi: 10.5004/dwt.2019.24360

162 (2019) 60–69
September

Purification of seawater by C–Cu–TiO_2 ceramic based membrane

Yasser A. Shaban[a,b,*], Mohamed I. Orif[a]

[a]*Marine Chemistry Department, Faculty of Marine Sciences, King Abdulaziz University, P.O. Box 80207, Jeddah 21589, Saudi Arabia, Tel. +966 595670522; emails: ydomah@kau.edu.sa/yasrsh@yahoo.com (Y.A. Shaban), mioraif@kau.edu.sa/morif99@yahoo.com (M.O. Orif)*
[b]*National Institute of Oceanography & Fisheries, Qayet Bay, Alexandria, Egypt*

Received 19 December 2018; Accepted 2 May 2019

ABSTRACT

In this study, a novel clay membrane coated with carbon–copper co-doped titanium oxide (C–Cu–TiO_2) nanoparticles was synthesized via sol-gel method. The membrane was evaluated in terms of purification of polluted seawater under illumination of UV and real sunlight by measuring some characteristic physical and chemical parameters such as, conductivity, salinity, nitrate (NO_3^-), nitrite (NO_2^-), ammonium (NH_4^+), chloride (Cl^-), phosphate (PO_4^{3-}), sulfate (SO_4^{2-}), sodium (Na^+), potassium (K^+), calcium (Ca^{2+}), magnesium (Mg^{2+}), total nitrogen (TN), and total organic carbon (TOC). Compared with pure TiO_2/clay, the C–Cu–TiO_2/clay membrane exhibited an excellent photocatalytic performance. The removal efficiency has been increased remarkably from 64.91% to 93.22% for TOC and from 36.92% to 68.94% for TN, when C–Cu–TiO_2/clay membrane was used, revealing its feasibility for the purification process. Moreover, the stability and potentiality of C–Cu–TiO_2/clay membrane for continuous reuse have been successfully demonstrated.

Keywords: Purification; Seawater; C–Cu–TiO_2; Clay; Membrane

1. Introduction

Globally, the problem of water scarcity is anticipated to grow in the coming years, due to the insufficient availability of clean water and deficiency of satisfactory water treatment. It is estimated that more than 1 billion people are exposed to unsafe drinking water source [1]. Particularly, this problem is significant in arid zones where water sources are scarce and in developing countries. The importance of seawater as a significant water source is globally increasing, since more than 70% of the earth's surface is covered by oceans, which contain 97% of the earth's water [2,3]. Therefore, the purification of seawater is an issue of significant environmental interest.

The limitations and drawbacks of traditional water treatment processes as well as the rigorous environmental standards have emerged the need to search for a novel water treatment technology to ensure sustainable production of high water quality. Accordingly, tremendous efforts have been devoted in the development of innovative and cost-effective modern treatment technologies to provide clean water. Recently, Intensive research has proven that solar photocatalysis technology utilizing photocatalyst nanoparticle can efficiently detoxify polluted water. Investigations included various photocatalysts, such as TiO_2 [4–9], WO_3 [10,11], Fe_2O_3 [12,13], CuS [14] and ZnO [15]. Due to its commercial viability, chemical stability, and environmentally benign properties, titanium oxide (TiO_2) has received great attention for environmental remediation. However, its wide bandgap (3.0–3.2 eV) requires UV light, of high energy, to excite electron in the valance band to conduction band, leaving a positive hole in the valance band, which is the key step in the photocatalysis mechanism. This hole can quickly recombine again with the electron resulting in a decline in

* Corresponding author.

the photoactivity of the catalyst. Thus, it is critical to modify the catalyst to overcome these two obstacles.

Recently, modification of *n*-TiO_2 photocatalyst by carbon proved to be an effective technique for reducing its optical bandgap [16], and successively, can absorb visible light photons [17–20]. Additionally; doping of TiO_2 by Cu(II) could improve its efficiency by suppressing the electron–hole recombination [21–26]. Concurrently, the doping by carbon can reduce the optical bandgap energy of TiO_2, and Cu-doping can overcome the recombination problem. Therefore, the co-doping of TiO_2 with both C and Cu is expected to facilitate and expedite the development of more sustainable processes for the remediation of contaminated water by efficient utilization of real solar light.

On the other hand, conventional inorganic membranes such as ceramic have shown some potential for the utilization as a physical tool for filtration and separation processes, due to its advantageous features such as, low capital cost, compact design, higher separation factors, excellent combinations of mechanical, chemical and thermal stability, and better cleaning properties [27]. Several methodologies have been proposed and addressed for the fabrication of composite membranes, including chemical vapor deposition [28], dip-coating [29], microwave-assisted hydrothermal treatment [30,31] and electroless plating [32]. In this context, fabrication of the membrane with cheap raw materials and lowering the temperature during sintering process would be beneficial to minimize the cost of the ceramic membranes and consolidate their industrial applications.

Due to their interesting simultaneous physical separation and chemical decomposition functions toward water contaminants and their promising practical applications [33,34], attention has been given to the fabrication of TiO_2 photocatalytic membranes. Therefore, the combination of physical purification tool with the photocatalysis technique employing visible light active nano-photocatalyst in a single unit will be of a great potential for purification technique. To the best of our knowledge, the application of combined inexpensive low-cost raw clay with C–Cu–TiO_2 nanoparticles to purify polluted seawater under natural sunlight has not been reported in the literature. Based on the aforementioned considerations, this work focused on the preparation of a clay membrane coated with carbon–copper co-doped titanium oxide (C–Cu–TiO_2) nanoparticles. The C–Cu–TiO_2/clay membrane was tested for the purification of polluted seawater under UV and real sunlight. The membrane performance was evaluated in terms of measuring of some characteristic physical and chemical parameters such as, conductivity, salinity, nitrate (NO_3^-), nitrite (NO_2^-), chloride (Cl^-), phosphate (PO_4^{3-}), sulfate (SO_4^{2-}), sodium (Na^+), potassium (K^+), calcium (Ca^{2+}), magnesium (Mg^{2+}), total nitrogen (TN) and total organic carbon (TOC).

2. Experimental

2.1. Preparation of the catalysts

C–Cu–TiO_2 nanoparticles were prepared via sol-gel method by the addition of titanium (IV) iso-propoxide (30 mL) to equal volume of absolute ethanol under continuous sonication. To achieve the incorporation of carbon and copper, 15 mL of mixture of sucrose (0.01 M) and copper sulfate (3 wt.%) were added into the prepared solution. Then the pH was adjusted to be around 3.2 and the sonication was maintained for 2 h to form the gel, which was kept for 24 h at room temperature and then dried at 100°C for 12 h. Finally, the obtained powder was calcined in a muffle furnace at 500°C for 2 h to attain the C–Cu–TiO_2 nanoparticles. Pure TiO_2 was prepared by following the same previously mentioned steps, without the addition of both sucrose and copper sulfate.

2.2. Preparation of ceramic support

Natural clay powder was provided from the local market of Jeddah, KSA. The clay was sieved to remove any large particles, then well grounded by using a ceramic mortar. A homogenous paste was made by using a milli-Q water, then the paste was made into small balls (with average dimensions of: 0.4 cm diameter, 1.3 cm circumference, and 0.538 cm^2 surface area) by using a homemade stainless steel circular shaped template. The formed wet clay balls were dried at room temperature for 24 h.

2.3. Characterization

X-ray diffraction (XRD) patterns were obtained by using an Ultima IV X-ray diffractometer (Rigaku, USA) with a copper K_α radiation at 40 mA and 40 kV, data collection was carried out over the 2θ range of 10°–80° at a scan rate of 4.0°min^{-1}. To study the morphology of the photocatalysts' surface, A JSM-7600F, JEOL (USA) scanning electron microscope (SEM) was used. Attached to this SEM, energy dispersive X-ray spectroscopic unit (EDS, X-max 50 mm^2, Oxford Instruments, USA), to perform the elemental composition and to examine the presence of carbon and copper in the photocatalysts. A Shimadzu, Pharma-Spec UV-1700 Spectrophotometer (USA) was used to record the UV–Vis spectra of the photocatalysts. To determine the chemical species at the surface of the photocatalyst, X-ray photoelectron spectroscopy (XPS) measurements were performed with a SPECS surface analysis systems operating at a base pressure of 4×10^{-10} mbar, using Mg–Kα (1,253.6 eV) X-ray source at 13.5 kV, 150 W of X-ray power.

2.4. Membrane design and purification experiments

A slurry of the synthesized photocatalyst (C–Cu–TiO_2 or TiO_2) was prepared by using Milli-Q water. The clay balls were immersed into the prepared slurry to be coated with a layer of the photocatalyst. Afterwards, the coated clay balls were dried at ambient temperature for 24 h, followed by heating in hot air oven at 100°C for 12 h, then calcinated in a muffle furnace at 500°C for 2 h.

The prepared C–Cu–TiO_2/clay and TiO_2/clay are then tightly packed in a Pyrex glass tube with the dimension of 20 cm length and 2 cm diameter to design C–Cu–TiO_2/clay and TiO_2/clay membranes. Additionally, a clay (without any casting catalyst) was designed to be employed as a reference membrane. Then each membrane is connected to the reaction vessel, containing clean seawater (CSW) or polluted seawater (PSW) samples (collected from Al-Arbaeen Lagoon and Sharm Obhur, Jeddah, KSA, respectively), with proper

tight tubing. A simple schematic representation of the reaction system is shown in Fig. 1. The system is operated with the help of a peristaltic pump (Cole-Parmer Instrument CO., Model 7014-20, USA), with a flow rate of 10 mL min^{-1}. UV lamps emitting 365 nm wavelength (Sankyo Denki, Germicidal Lamp, G15 T8-Japan) were used to irradiate the membrane from all sides. To perform the solar photocatalytic experiments, the membrane was directly exposed to the real sunlight during the periods from 09:30 am to 2:30 pm of the sunny days. The average solar intensity, measured by a 3670i Silicon Pyranometer Sensor attached to Field Scout Light Sensor Reader (Spectrum Technologies, Inc., USA) found to be 1,200 W m^{-2}.

Treated samples were withdrawn at equal intervals of time and were analyzed. Nitrogen and phosphorus species were determined by conventional colorimetric method by using Shimadzu-UV-2450 spectrophotometer, according to Grasshoff et al. [35]. A Shimadzu total organic carbon analyzer (TOC-V_{CPH}) was used for measuring the total organic carbon (TOC), whereas the total nitrogen (TN) was analyzed by total nitrogen unit (TNM-1) attached to TN analyzer (Shimadzu-V_{CPH}). Salinity and conductivity were measured by CLEAN CON500 conductivity/salinity meter. Na, K and Ca were measured by Jenway Flame Photometer-Model PFP7 (UK). Titration method was applied for the determination of Mg [35,36]. Finally, sulfate was analyzed according the turbidimetric method [37] by using Shimadzu UV-2450 spectrophotometer.

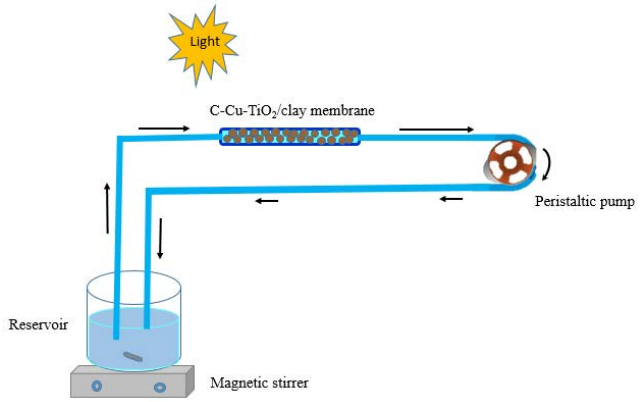

Fig. 1. Schematic diagram of experimental setup.

3. Results and discussion

3.1. Characterization

Fig. 2 exhibits the XRD patterns of the raw clay, pure TiO_2 and C–Cu–TiO_2. The characteristic diffraction peaks of the raw clay showed the presence of quartz, K-feldspar, plagioclase feldspar and clay minerals (Fig. 2a). Only a typical pattern of anatase phase was found for both TiO_2 and C–Cu–TiO_2 (Fig. 2b). No characteristic peaks of Cu or C were shown for C–Cu–TiO_2, which may be due to their complete incorporation into the crystal lattice of TiO_2 or their high dispersion over TiO_2 surface [38]. The crystal sizes of TiO_2 and C–Cu–TiO_2 were found to be 18.6 nm, respectively, as calculated by using the Scherrer equation, $D = 0.9\,\lambda/(\beta\cos\theta)$, where λ stands for wavelength of X-ray (0.1541 nm), β is the full width at half maximum (FWHM), θ is the diffraction angle and D is the mean crystallite size (nm).

The morphological characteristics of C–Cu–TiO_2 and TiO_2 are shown by the SEM images (Fig. 3). A typical spherical, nanosized particles for both C–Cu–TiO_2 and TiO_2 are clearly noted. The elemental composition determined through EDS analysis evidenced the doping of C and Cu in Cu–C–TiO_2 with atomic% of 36.13, 51.94, 11.00 and 0.93 for Ti, O, C and Cu, respectively (Fig. 4b). Whereas the atomic% of Ti and O for pure TiO_2 were found to be 34.36 and 65.64, respectively (Fig. 4a).

Obviously, the optical band gap has been reduced from 2.99 eV for pure TiO_2 to 1.77 eV for C–Cu–TiO_2 upon doping by C and Cu, as clearly demonstrated in Fig. 5, by the Tauc plot of transformed Kubelka–Munk function [39,40]. The observed reduction in the band gap of C–Cu–TiO_2 can be attributed to the mixing of O 2p states with C 2p states, where, C 2p can act as an acceptor state, as a result of the lower number of electrons in the valence shell of the dopant C atom than the valence shell electron numbers of O in TiO_2 [41]. On the other hand, the higher positive reduction potential of Cu ions than the conduction band edge of TiO_2 (≈ –0.2 V), and the strong interaction between the implanted

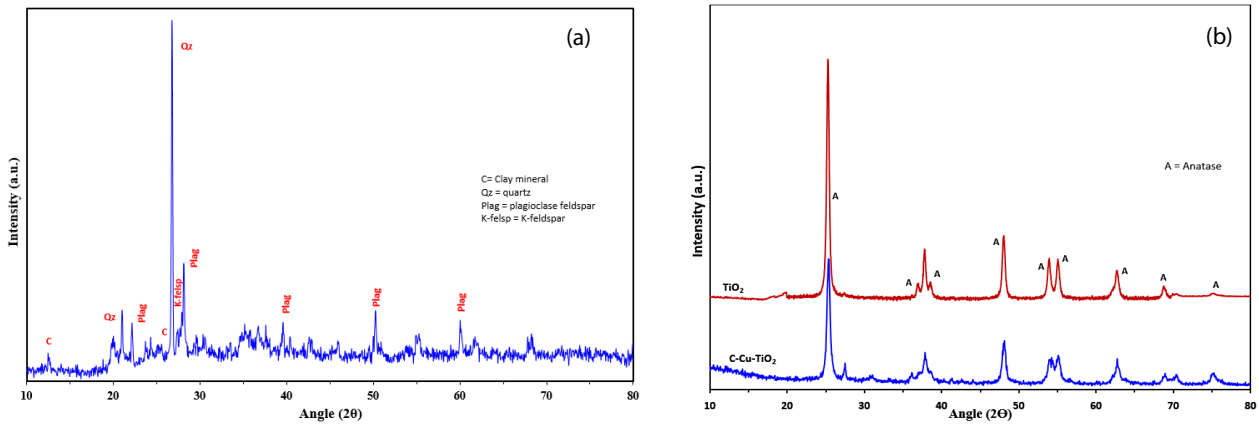

Fig. 2. XRD patterns for (a) raw clay and (b) pure TiO_2 and C–Cu–TiO_2.

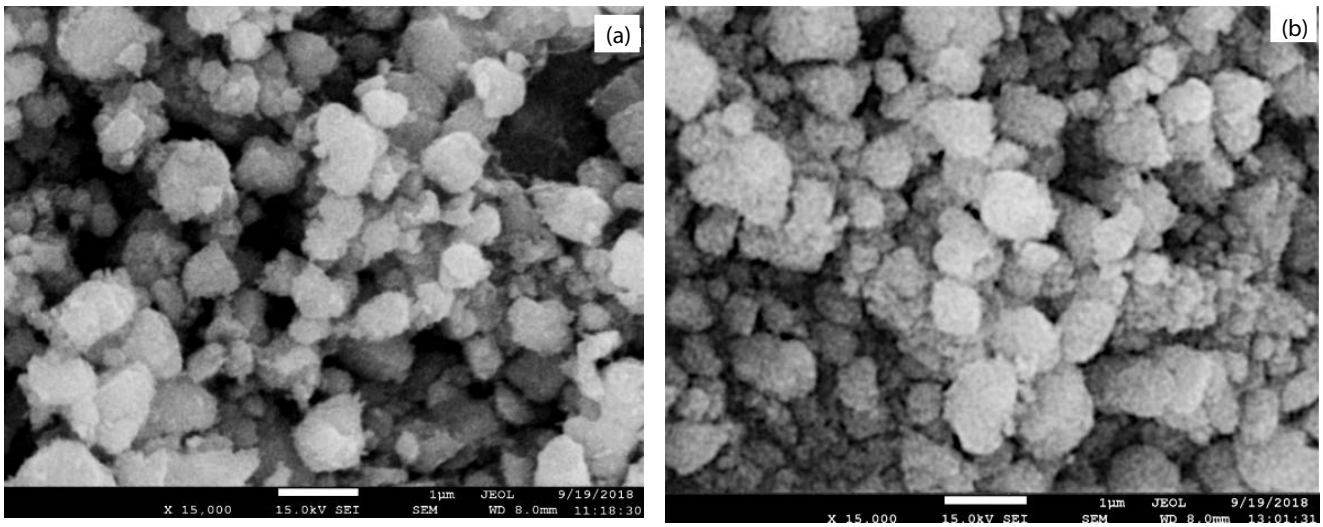

Fig. 3. SEM images for (a) pure TiO_2 and (b) C–Cu–TiO_2.

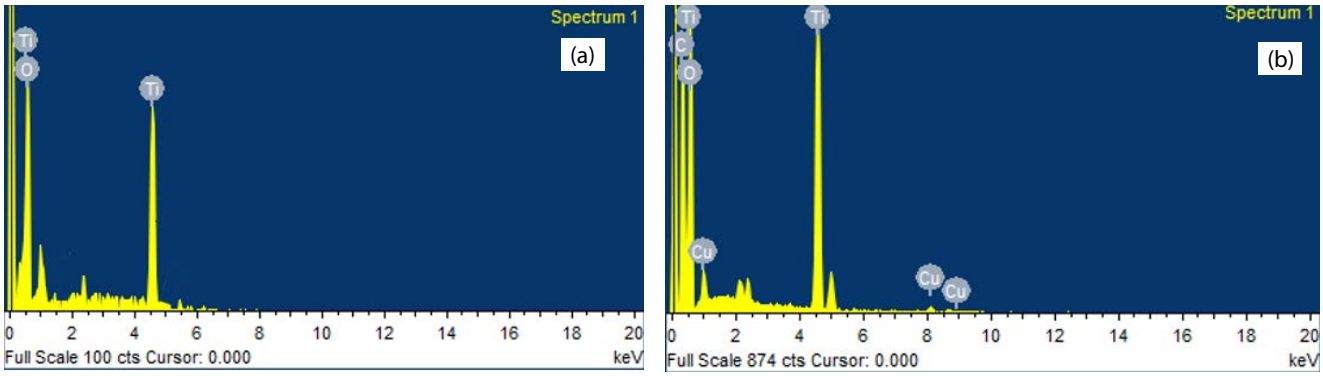

Fig. 4. EDS analysis for (a) pure TiO_2 and (b) C–Cu–TiO_2.

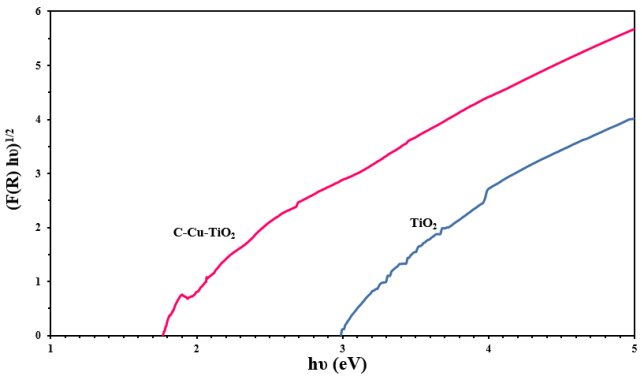

Fig. 5. Transformed Kubelka–Munk function plot for pure TiO_2 and C–Cu–TiO_2.

dopant Cu ions and TiO_2 increase the feasibility of trapping an electron by Cu ions within the semiconductor photocatalyst, therefore, Cu dopant can effectively act as an electron trapper to prohibit electron–hole recombination.

XPS analysis was performed to determine the chemistry of the atoms in C–Cu–TiO_2 (Fig. 6). The XPS survey spectrum in Fig. 6a confirmed the existence of Ti, O, C and Cu species. The Ti 2p spectrum in Fig. 6b indicates XPS peaks at about 457.1 eV (Ti $2p_{3/2}$) and 464.2 eV (Ti $2p_{1/2}$) both of which are ascribed to Ti^{4+}. There are other two peaks at 458.6 eV (Ti $2p_{3/2}$) and 462.2 eV (Ti $2p_{1/2}$) which can be attributed to Ti^{3+} oxidation state [42]. The XPS spectra for O 1s (Fig. 6c) exhibited a major peak at around 530.2 eV corresponding to lattice oxygen O^{2-} in TiO_2 (Ti–O, Ti–O–Ti). The other two peaks at about 532.1 and 534.1 eV can be ascribed to the chemisorbed oxygen or the surface free hydroxyl group (O–H) [43–45]. The XPS spectra of C 1s (Fig. 4d) indicated four peaks. The first peak at approximately 283.3 eV can be assigned to C–Cu, while the other three peaks with binding energies located at about 285.2, 286.9 and 288.8 eV can be ascribed to C–C, C–O/C=O and O–C=O, respectively [43,46–48]. The XPS spectra for Cu $2p_{3/2}$ appeared at 933.1 and 935.9 eV (Fig. 6e), indicating the presence of copper as Cu^{2+} [48,49].

3.2. Photocatalytic purification

3.2.1. Salinity

Salinity is the amount of dissolved solids in seawater and used for determining the density of seawater. According to WHO guidelines [50], the water with a total dissolved

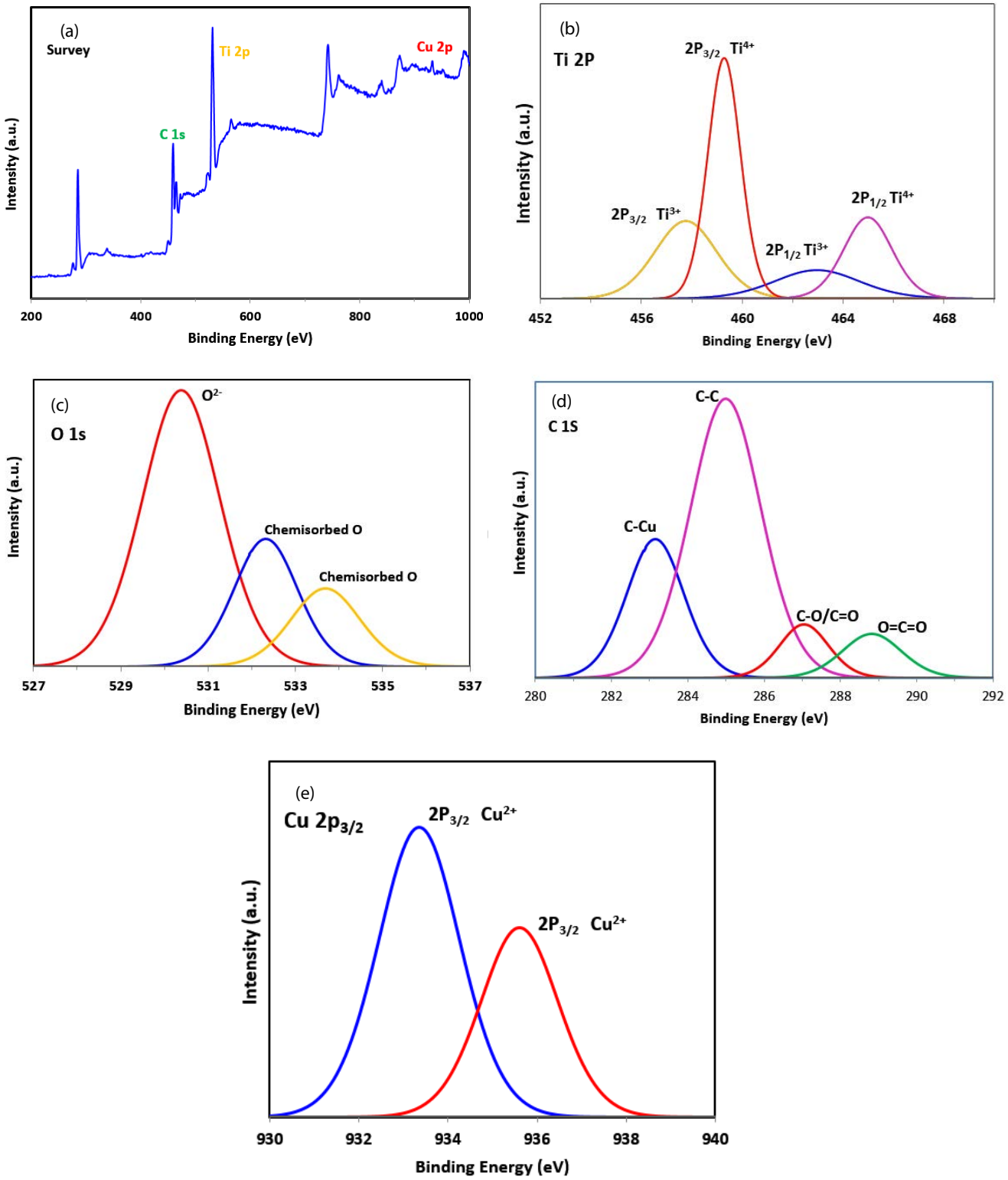

Fig. 6. X-ray photoelectron spectroscopy (XPS) for (a) survey, (b) Ti 2p, (c) O 1S, (d) C 1S, and (e) Cu 2p3/2 for C–Cu–TiO_2.

solid level of less than about 600 mg L^{-1} is generally considered to be good. The ability of C–Cu–TiO_2/clay membrane to reduce the dissolved solids in seawater is clearly noted as can be seen from Fig. 7. The salinity of CSW has been remarkably reduced from 38.71 ppt to 26.2 and 24.7 ppt, under UV and real sunlight illumination, respectively. Similar reduction was also observed for PSW, which has lower salinity of 19.12 ppt due to the discharge of wastewater, to the value

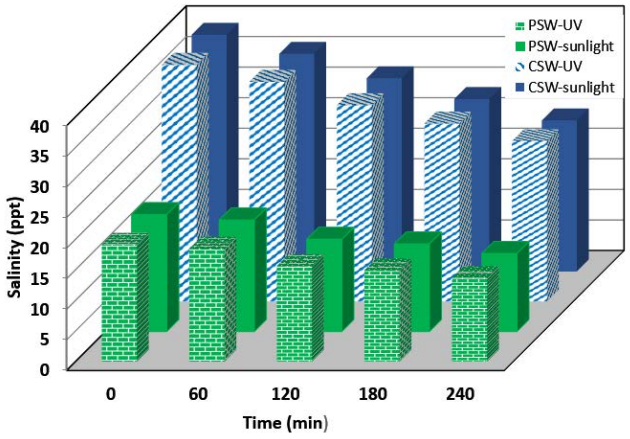

Fig. 7. Variations of salinity of CSW and PSW with C–Cu–TiO_2/clay membrane treatment time under UV and real sunlight illumination.

of 13.65 ppt under illumination of UV and 12.76 ppt under natural sunlight.

3.2.2. Total organic carbon

Total organic carbon (TOC) is the amount of carbon bound in an organic compound and it is often used as a nonspecific indicator of water quality [51]. Therefore, the extent of mineralization and the degradation of the intermediates can be estimated by measuring the concentration of TOC, which in turn can be used as a tool for evaluating the performance of the C–Cu–TiO_2/clay membrane. It is clearly seen that 83.1% and 99.5% elimination efficiencies of 4.46 mg L^{-1} of TOC from CSW have been achieved by using C–Cu–TiO_2/clay membrane after 4 h of irradiation under UV and sunlight, respectively (Fig. 8a). Whereas the membrane mineralization efficiency reached 81.9% and 93.2% of 27.62 mg L^{-1} of TOC presented in PSW after the same illumination time under UV and sunlight, respectively (Fig. 8b), evidencing the effectiveness and capability of the membrane for mineralization and degradation of TOC even in polluted seawater.

3.2.3. Nutrients and total nitrogen (TN)

The inputs of nutrients into seawater can be considered beneficial for the production of fish and shellfish [52]. However, excess nutrients can be highly damaging, leading to effects such as hypoxia and anoxia from eutrophication, nuisance algal blooms, dieback of sea grasses and corals and reduced population of fish and shellfish [53]. The efficient removal of nutrients; nitrate (NO_3^-), nitrite (NO_2^-), ammonium (NH_4^+) and phosphate (PO_4^{3-}) from CSW and PSW samples using the C–Cu–TiO_2/clay membrane is clearly demonstrated in Figs. 9a and b, respectively.

Total nitrogen is the sum of total Kjeldahl nitrogen (ammonia, organic and reduced nitrogen) and nitrate–nitrite. An excess amount of nitrogen in a water resources may lead to low levels of dissolved oxygen and negatively alter various plant life and organisms. Fig. 9c shows the variation of observed total nitrogen (TN) values in the treated CWS and PSW samples by using the C–Cu–TiO_2/clay membrane with respect to UV and sunlight illumination time. It shows a remarkable reduction of TN value presented in PSW from 39.61 to 20.11 μM (under UV) and 12.3 μM (under sunlight).

3.2.4. Cations, anions and conductivity

Table 1 shows the analysis of cations (Na^+, K^+, Ca^{2+} and Mg^{2+}) and anions (SO_4^{2-} and Cl^-) in CSW and PSW samples with respect to irradiation time under UV and real sunlight. The effective photocatalytic removal of cations and anions by using the C–Cu–TiO_2/clay membrane is clearly noted. For all analyzed elements, solar light assisted removal efficiencies are higher than those observed under UV light, revealing the ability of the membrane for harvesting the maximum solar photons.

Conductivity is the measure of the capability of water to pass electrical flow, which is directly related to the concentration of ions in water [54]. These conductive ions come from dissolved salts and inorganic materials such as chlorides, sulfides, carbonate compounds and alkalis [55,56]. The more ions that are present, the higher the conductivity of water. Conductivity is considered to be one of the most valuable and commonly measured water quality parameters as it is an early indicator of change in a water system [55,56]. A sudden

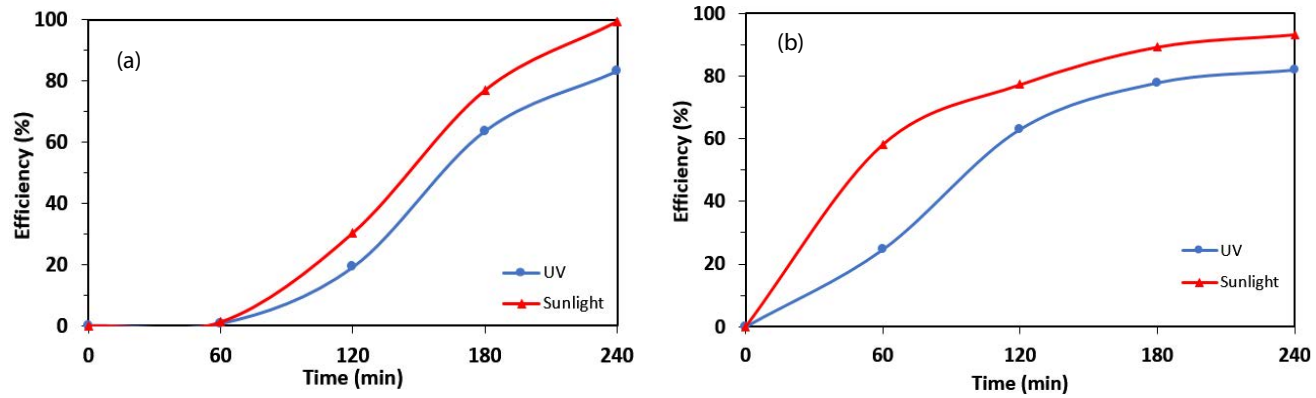

Fig. 8. Removal efficiency of total organic carbon (TOC) by using C–Cu–TiO_2/clay membrane under UV and real sunlight illumination from (a) CSW and (b) PSW.

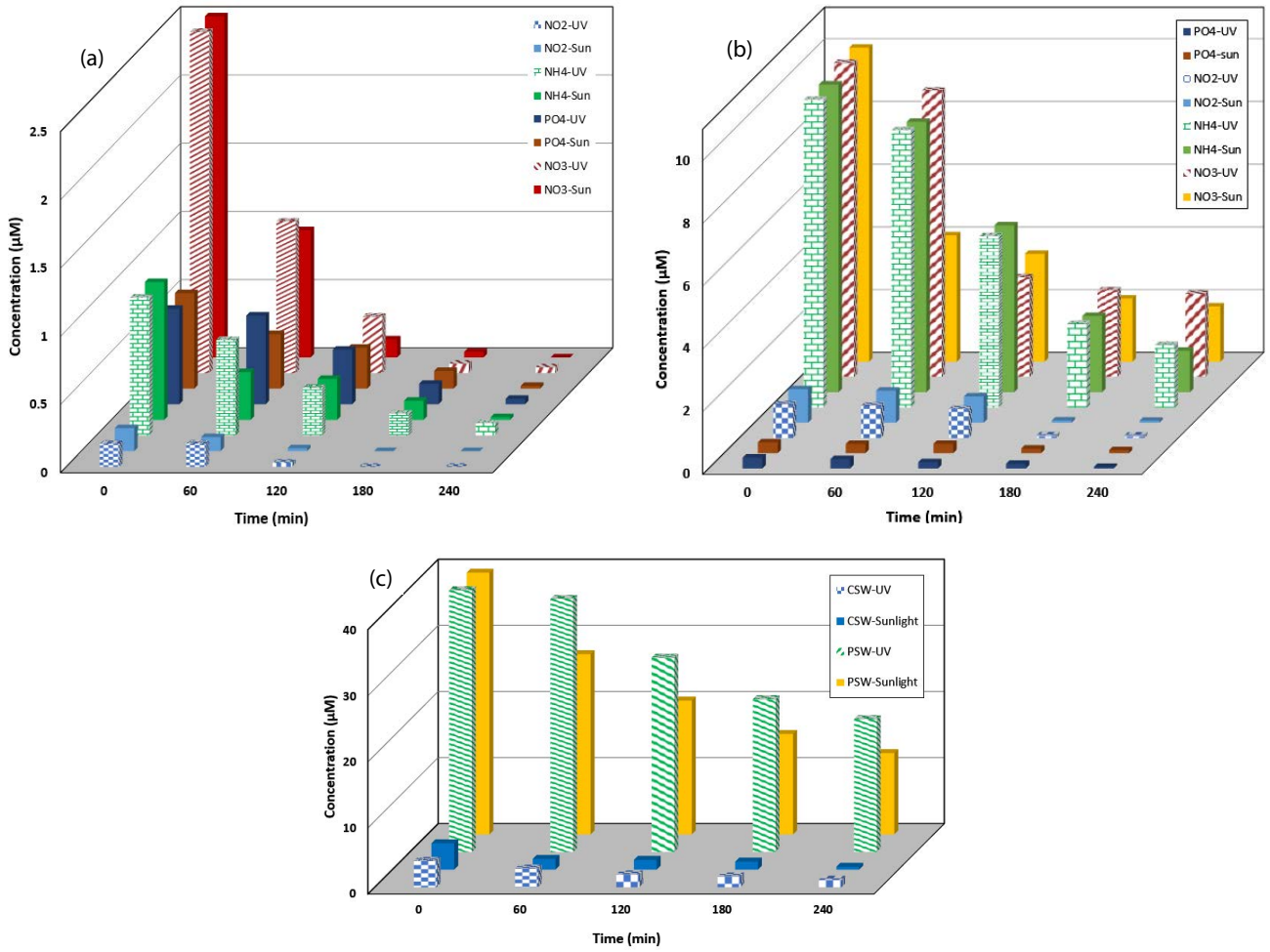

Fig. 9. Removal of: (a) nutrients from CSW, (b) nutrients from PSW, and (c) total nitrogen from CSW and PSW by using C–Cu–TiO_2/clay membrane under UV and real sunlight illumination.

Table 1
Analysis of cations and anions in CSW and PSW samples treated with C–Cu–TiO_2/clay membrane with respect to irradiation time under UV and real sunlight

Time (min)		0		60		120		180		240	
		CSW	PCW	CSW	PCW	CSW	PCW	CSW	PCW	CSW	PCW
Na (mg L^{-1})	UV	11,836.00	5,865	11,837.00	5,099	11,838.00	4,345	11,839.00	3,404	11,623	2,877
	Sunlight	11,836.00	5,865	9,908.8	4,158	8,531.1	3,723	6,408.5	3,142	5,543	2,318
K (mg L^{-1})	UV	438.00	211.0	399.00	193.6	378.00	153.7	330.00	128.3	312	101.1
	Sunlight	438.00	211.0	363.0	181.9	272.4	160.95	174.7	109.52	75	77.9
Ca (mg L^{-1})	UV	454.00	217.0	455.00	213.8	456.00	161.5	457.00	130.6	454	75.7
	Sunlight	454.00	217.0	388.6	190.2	352.2	154.8	298.3	106.6	225	67.6
Mg (mg L^{-1})	UV	1,869.05	675.0	1,810.72	659.2	1,694.06	652.7	1,531.22	623.8	1,465	601.2
	Sunlight	1,869.05	675.0	1,776.3	644.6	154.0	613.2	1,382.3	557.6	1,174	501.2
SO_4 (mg L^{-1})	UV	2,990.00	1,350.0	2,816.45	1,151.6	1,962.58	956.7	1,309.08	700.2	765	655.4
	Sunlight	2,990.00	1,350.0	2,622.2	1,131.6	1,518.7	825.9	1,162.8	619.4	439.1	423.2
Cl (mg L^{-1})	UV	21,428.18	10,584.0	19,878.22	10,218.7	17,769.17	8,635.5	16,108.50	8,253.5	15,441	7,899.3
	Sunlight	21,428.18	10,584.0	19,701.1	10,090.5	17,492.4	8,347.63	15,615.8	7,926.27	14,357	6,632.1

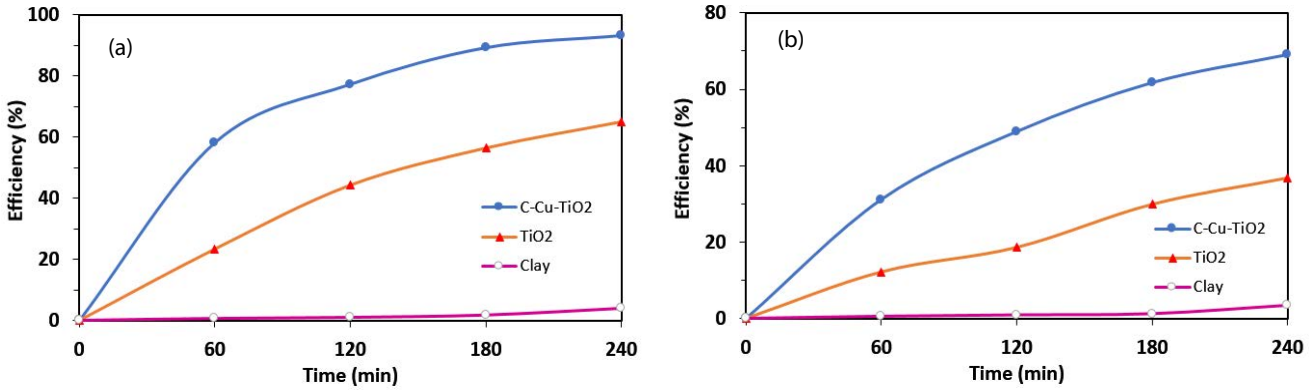

Fig. 10. Removal efficiency of (a) TOC and (b) TN by using clay, TiO_2/clay and C–Cu–TiO_2/clay membranes under real sunlight illumination.

increase or decrease in conductivity in a body of water can indicate pollution. Unusual conductivity and salinity levels are usually indicative of pollution [54].

It is worthy noted that the conductivity of CSW sample has been decreased from 59.7 mS cm^{-1} to 34.79 and 32.65 mS cm^{-1} under illumination of UV and sunlight, respectively. Due to the dilution of the ions concentration as a result of the sewage discharge, the conductivity of polluted seawater sample recoded a lower value of 19.12 mS cm^{-1} which has been reduced after 4 h of photocatalytic treatment under UV and sunlight to the values of 13.65 and 12.76 mS cm^{-1}, respectively.

3.3. Performance of C–Cu–TiO_2/clay membrane

The performance of C–Cu–TiO_2/clay membrane was comparatively evaluated with both pure TiO_2/clay and the clay (without any catalyst) membranes under the same experimental conditions. The removal of TOC (27.62 mg L^{-1}) and TN (3.98 μM) from PSW was used as a model to evaluate the performance of C–Cu–TiO_2/clay membrane under natural sunlight (Fig. 10). When the clay membrane was applied without any coating catalyst, only 4.2% and 3.4% removal efficiencies were observed for TOC and TN, respectively, which can be attributed to the adsorption process. The removal efficiency increased to 64.91% for TOC and 36.92% for TN, when the pure TiO_2/clay membrane was utilized. Significantly, the photocatalytic elimination efficiency using C–Cu–TiO_2/clay membrane has been enhanced to 93.22% and 68.94% for TOC and TN, respectively. These results reflect the high capability of C–Cu–TiO_2/clay membrane for the purification process, as a result of the combination of physical purification tool, adsorption process by the clay, with the photocatalysis technique employing visible light active C–Cu–TiO_2 nano-photocatalyst in a single unit.

3.4. Reusability of the membrane

Reusability is one of the most significant parameters in designing, economic viability and practical applicability of a membrane in large-scale. The reusability of the membrane was evaluated over three consecutive repetitions. The measurements of TOC and TN were used to assess the ability of the membrane to reproduce the same measurements (Fig. 11). The consistency of the results obtained after the three attempts is clearly noted. Less than 1.0% loss was observed for the removal efficiency of both TOC and TN from PSW under natural sunlight, revealing the potentiality of the membrane for continuous reuse.

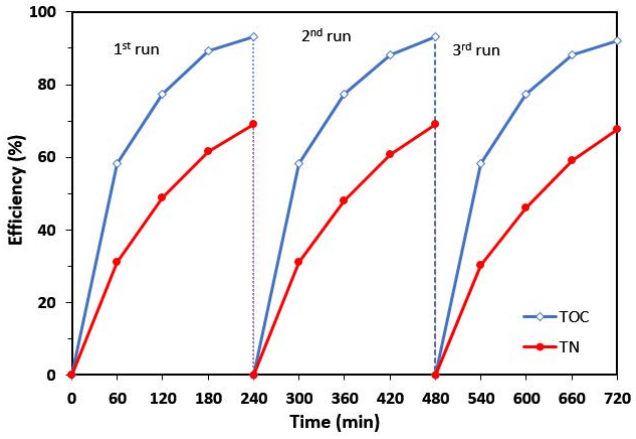

Fig. 11. Cyclic photocatalytic removal of TOC and TN by using C–Cu–TiO_2/clay membrane under real sunlight illumination.

4. Conclusions

C–Cu–TiO_2/clay membrane was synthesized and evaluated in terms of purification of polluted seawater under UV and real sunlight. The purification tests of this membrane have given promising results by measuring some characteristic physical and chemical parameters such as conductivity, salinity, nitrate (NO_3^-), nitrite (NO_2^-), chloride (Cl^-), phosphate (PO_4^{3-}), sulfate (SO_4^{2-}), sodium, potassium, calcium, magnesium, total nitrogen and total organic carbon (TOC). The feasibility for excellent purification performance by C–Cu–TiO_2/clay membrane has been clearly demonstrated through the comparison with the pure TiO_2/clay. The removal efficiency has been enhanced significantly from 64.91% for TOC and 36.92% for TN, when pure TiO_2/clay was used to 93.22% for TOC and 68.94% for TN by using C–Cu–TiO_2/

clay membrane. Furthermore, the stability and reusability of C–Cu–TiO_2/clay membrane have been successfully achieved.

Acknowledgments

This project was funded by the Deanship of Scientific Research (DSR) at King Abdulaziz University, Jeddah, under grant no. G-315-150-38. The authors, therefore, acknowledge with thanks DSR for technical and financial support. The authors would like to thank Mr. Mosa Alzobidi and Dr. Yasar N. Kavil for their appreciable help in the experimental analysis.

References

[1] World Health Organization (WHO), UNICEF, Global Water Supply and Sanitation Assessment 2000 Report, WHO, Geneva, Switzerland, 2000.
[2] A.T. Wolf, Water and human security, J. Contemp. Water Res. Educ., 118 (2001) 29–37.
[3] World Health Organization (WHO), Guidelines for Drinking Water Quality, Surveillance and Control of Community Supplies, Vol. 3, 2nd ed., WHO, Geneva, 1997.
[4] S. Yang, J.-S. Gu, H.-Y. Yu, J. Zhou, S.-F. Li, X.-M. Wu, L. Wang, Polypropylene membrane surface modification by RAFT grafting polymerization and TiO_2 photocatalysts immobilization for phenol decomposition in a photocatalytic membrane reactor, Sep. Purif. Technol., 83 (2011) 157–165.
[5] R. Mu, Z. Xu, L. Li, Y. Shao, H. Wan, S. Zheng, On the photocatalytic properties of elongated TiO_2 nanoparticles for phenol degradation and Cr(VI) reduction, J. Hazard. Mater., 176 (2010) 495–502.
[6] N.M. Mahmoodi, M. Arami, N.Y. Limaee, Photocatalytic degradation of triazinic ring-containing azo dye (Reactive Red 198) by using immobilized TiO_2 photoreactor: bench scale study, J. Hazard. Mater., 133 (2006) 113–118.
[7] Y. Zhang, D. Wang, G. Zhang, Photocatalytic degradation of organic contaminants by TiO_2/sepiolite composites prepared at low temperature, Chem. Eng. J., 173 (2011) 1–10.
[8] H.A. Le, L.T. Linh, S. Chin, J. Jurng, Photocatalytic degradation of methylene blue by a combination of TiO_2-anatase and coconut shell activated carbon, Powder Technol., 225 (2012) 167–175.
[9] S.-y. Lu, D. Wu, Q.-l. Wang, J. Yan, A.G. Buekens, K.-f. Cen, Photocatalytic decomposition on nano-TiO_2: destruction of chloroaromatic compounds, Chemosphere, 82 (2011) 1215–1224.
[10] H. Lee, J. Choi, S. Lee, S.-T. Yun, C. Lee, J. Lee, Kinetic enhancement in Photocatalytic oxidation of organic compounds by WO_3 in the presence of Fenton-like reagent, Appl. Catal., B, 138–139 (2013) 311–317.
[11] X. Gao, X. Su, C. Yang, F. Xiao, J. Wang, X. Cao, S. Wang, L. Zhang, Hydrothermal synthesis of WO_3 nanoplates as highly sensitive cyclohexene sensor and high-efficiency MB photocatalyst, Sens. Actuators, B, 181 (2013) 537–543.
[12] Z. Miao, S. Tao, Y. Wang, Y. Yu, C. Meng, Y. An, Hierarchically porous silica as an efficient catalyst carrier for high performance vis-light assisted Fenton degradation, Microporous Mesoporous Mater., 176 (2013) 178–185.
[13] Y.J. Zhang, L.C. Liu, L.L. Ni, B.L. Wang, A facile and low-cost synthesis of granulated blast furnace slag-based cementitious material coupled with Fe_2O_3 Catalyst for treatment of dye wastewater, Appl. Catal., B, 138–139 (2013) 9–16.
[14] V.K. Gupta, D. Pathania, S. Agarwal, P. Singh, Adsorptional photocatalytic degradation of methylene blue onto pectin-CuS nanocomposite under solar light, J. Hazard. Mater., 243 (2012) 179–186.
[15] S. Liu, X. Wang, W. Zhao, K. Wang, H. Sang, Z. He, Synthesis, characterization and enhanced photocatalytic performance of Ag_2S-coupled ZnO/Zn Score/shell nanorods, J. Alloys Compd., 568 (2013) 84–91.
[16] S.U.M. Khan, M. Al-Shahry, W.B. Ingler Jr., Efficient photochemical water splitting by a chemically modified n-TiO_2, Science, 297 (2002) 2243–2245.
[17] Y.A. Shaban, S.U.M. Khan, Visible light active carbon modified *n*-TiO_2 for efficient hydrogen production by photoelectrochemical splitting of water, Int. J. Hydrogen Energy, 33 (2008) 1118–1126
[18] C. Xu, R. Killmeyer, M.L. Gray, S.U.M. Khan, Photocatalytic effect of carbon-modified *n*-TiO_2 nanoparticles under visible light illumination, Appl. Catal., B, 64 (2006) 312–317.
[19] Y.A. Shaban, A.A. El Maradny, R.K. Al Farawati, Photocatalytic reduction of nitrate in seawater using C/TiO_2 nanoparticles, J. Photochem. Photobiol., A, 328 (2016) 114–121.
[20] Y.A. Shaban, M.A. El Sayed, A.A. El Maradny, R.Kh. Al Farawati, M.I. Al Zobidi, Photocatalytic degradation of phenol in natural seawater using visible light active carbon modified (CM)-n-TiO_2 nanoparticles under UV light and natural sunlight illuminations, Chemosphere, 91 (2013) 307–313.
[21] M. Anpo, H. Yamashita, Y. Ichihashi, Y. Fujii, M. Honda, Photocatalytic reduction of CO_2 with H_2O on titanium oxides anchored within micropores of zeolites: effects of the structure of the active sites and the addition of Pt, J. Phys. Chem. B, 101 (1997) 2632–2636.
[22] H. Yamashita, H. Nishiguchi, N. Kamada, M. Anpo, Y. Teraoka, H. Hatano, M. Sciavello, Photocatalytic reduction of CO_2 with H_2O on TiO_2 and Cu/TiO_2 catalysts, Res. Chem. Intermed., 20 (1994) 815–823.
[23] K. Adachi, K. Ohta, T. Mizuno, Photocatalytic reduction of carbon dioxide to hydrocarbon using copper-loaded titanium dioxide, Sol. Energy, 53 (1994) 187–190.
[24] N. Sasirekha, S.J.S. Basha, K. Shanthi, Photocatalytic performance of Ru doped anatase mounted on silica for reduction of carbon dioxide, Appl. Catal., B, 62 (2006) 169–180.
[25] M. Tahir, N.S. Amin, Indium-doped TiO_2 nanoparticles for photocatalytic CO_2 reduction with H_2O vapors to CH_4, Appl. Catal., B, 162 (2015) 98–109.
[26] M.R. Uddin, M.R. Khan, M.W. Rahman, A. Yousuf, C.K. Cheng, Photocatalytic reduction of CO_2 into methanol over $CuFe_2O_4$/TiO_2 under visible light irradiation, React. Kinet. Mech. Catal., 116 (2015) 589–604.
[27] P. Monash, G. Pugazhenthi, Development of ceramic supports derived from low-cost raw materials for membrane applications and its optimization based on sintering temperature, Int. J. Appl. Ceram. Technol., 8 (2011) 227–238.
[28] M. Amanipour, A. Safekordi, E.G. Babakhani, A. Zamaniyan, M. Heidari, Effect of synthesis conditions on performance of a hydrogen selective nano-composite ceramic membrane, Int. J. Hydrogen Energy, 37 (2012) 15359–15366.
[29] I. Erdem, M. Ciftcioglu, S. Harsa, Separation of whey components by using ceramic composite membranes, Desalination, 189 (2006) 87–91.
[30] A. Huang, Y.S. Lin, W. Yang, Synthesis and properties of A-type zeolite membranes by secondary growth method with vacuum seeding, J. Membr. Sci., 245 (2004) 41–51.
[31] Y. Li, H. Chen, J. Liu, W. Yang, Microwave synthesis of LTA zeolite membranes without seeding, J. Membr. Sci., 277 (2006) 230–239.
[32] R. Sari, Z. Yaakob, M. Ismail, W.R.W. Daud, L. Hakim, Palladium–alumina composite membrane for hydrogen separator fabricated by combined sol–gel, and electroless plating technique, Ceram. Int., 39 (2013) 3211–3219.
[33] H. Choi, E. Stathatos, D.D. Dionysiou, Sol-gel preparation of mesoporous photocatalytic TiO_2 films and TiO_2/Al_2O_3 composite membranes for environmental applications, Appl. Catal., B, 63 (2006) 60–67.
[34] M.A. Anderson, M.J. Gieselmann, Q. Xu, Titania and alumina ceramic membranes, J. Memb. Sci., 39 (1988) 243–258.
[35] K. Grasshoff, K. Kremling, M. Erhardt, Methods of Seawater Analysis, Welly-VCH, Weinheim, New York, 1999.
[36] J.D. Strickland, T.R. Parsons, A Practical Handbook of Seawater Analysis, Fisheries Research Board of Canada, Ottawa, 1972.
[37] American Public Health Association (APHA), Standard Methods for Examination of Water and Wastewater, 14th ed., New York, 1976.

[38] V.K.K. Tangirala, H. Gómez-Pozos, V. Rodríguez-Lugo, M.D.L.L. Olvera, A study of the CO sensing responses of Cu-, Pt- and Pd-activated SnO_2 sensors: effect of precipitation agents, Dopants and Doping Methods, Sensors, 17 (2017) 1011–1035.
[39] P. Kubelka, New contributions to the optics of intensely light-scattering materials. Part I., J. Opt. Soc. Am., 38 (1948) 448–457.
[40] T. Tauc, R. Grigorovici, A. Vancu, Optical properties and electronic structure of amorphous germanium, Phys. Status Solidi B, 15 (1966) S627–637.
[41] Y. Nakano, T. Morikawa, T. Ohwaki, Y. Taga, Electrical characterization of band gap states in C-doped TiO_2 films, Appl. Phys. Lett., 87 (2005), doi.org/10.1063/1.2008376.
[42] Y.G. Tao, Y.Q. Xu, J. Pan, H. Gu, C.Y. Qin, P. Zhou, Glycine assisted synthesis of flower-like TiO_2 hierarchical spheres and its application in photocatalysis, Mater. Sci. Eng., B, 177 (2012) 1664–1671.
[43] G. Zhang, Y.C. Zhang, M. Nadagouda, C. Han, K. O'Shea, S.M. El-Sheikh, A.A. Ismail, D.D. Dionysiou, Visible light-sensitized S, N and C co-doped polymorphic TiO_2 for photocatalytic destruction of microcystin-LR, Appl. Catal., B, 144 (2014) 614–621.
[44] V. Trevisan, A. Olivo, F. Pinna, M. Signoretto, F. Vindigni, G. Cerrato, C.L. Bianchi, C-N/TiO_2 photocatalysts: effect of co-doping on the catalytic performance under visible light, Appl. Catal., B, 160 (2014) 152–160.
[45] S.M. El-Sheikh, G. Zhang, H.M. El-Hosainy, A.A. Ismail, K.E. O'Shea, P. Falaras, A.G. Kontos, D.D. Dionysiou, High performance sulfur, nitrogen and carbon doped mesoporous anatase–brookite TiO_2 photocatalyst for the removal of microcystin-LR under visible light irradiation, J. Hazard. Mater., 280 (2014) 723–733.
[46] X.F. Lei, X.X. Xue, H. Yang, C. Chen, X. Li, M.C. Niu, X.Y. Gao, Y.T. Yang, Effect of calcination temperature on the structure and visible-light photocatalytic activities of (N, S and C) co-doped TiO_2 nano-materials, Appl. Surf. Sci., 332 (2015) 172–180.
[47] V. Etacheri, M. Seery, S. Hinder, G. Michlits, S. Pillai, A highly efficient $TiO_{2-x}C_x$ nano-heterojunction photocatalyst for visible light induced antibacterial applications, ACS Appl. Mater. Interfaces, 5 (2013) 1663–1672.
[48] X. Guo, D. Mao, G. Lu, S. Wang, G. Wu, The influence of La doping on the catalytic behavior of Cu/ZrO_2 for methanol synthesis from CO_2 hydrogenation, J. Mol. Catal. A: Chem., 345 (2011) 60–68.
[49] L.C. Wang, Q. Liu, M. Chen, Y.M. Liu, Y. Cao, H.Y. He, K.N. Fan, Structural evolution and catalytic properties of nanostructured Cu/ZrO_2 catalysts prepared by oxalate gel-coprecipitation technique, J. Phys. Chem. C, 111 (2007) 16549–16557.
[50] WHO Expert Committee on Biological Standardization, Meeting and World Health Organization, WHO Expert Committee on Biological Standardization: 63rd Report, Vol. 980, World Health Organization, Geneva, Switzerland, 2013.
[51] F. Shahrezaei, Y. Mansouri, A.A.L. Zinatizadeh, A. Akhbari, Photocatalytic degradation of aniline using TiO_2 nanoparticles in a vertical circulating photocatalytic reactor, Int. J. Photoenergy, 2012 (2012) 8 p, doi.org/10.1155/2012/430638.
[52] S.W. Nixon, Physical energy inputs and the comparative ecology of lake and marine ecosystems, Limnol. Oceanogr., 33 (1988) 1005–1025.
[53] S.P. Baden, The cryptofauna of *Zostera marina* (L.): abundance, biomass and population dynamics, Netherlands J. Sea Res., 27 (1990) 81–92.
[54] R.G. Wetzel, Limnology: Lake and River Ecosystems, 3rd ed., Academic Press, San Diego, CA, 2001.
[55] EPA (2012), Conductivity in Water: Monitoring and Assessment, 2018. Available at: http://water.epa.gov/type/rsl/monitoring/vms59.cfm.
[56] R.L. Miller, W.L. Bradford, N.E. Peters, Specific Conductance: Theoretical Considerations and Application to Analytical Quality Control, In: U.S. Geological Survey Water-Supply Paper, 1988, Available at: http://pubs.usgs.gov/wsp/2311/report.pdf. (Visiting date: 10.10.2018).